









RESEARCH ARTICLE | JULY 26 2024

## Non-equilibrium and self-organization evolution in hot-spot ignition processes

X.-Y. Fu ; Z.-Y. Guo ; Q.-H. Wang ; R.-C. Wang ; D. Wu  ; J. Zhang  



*Phys. Plasmas* 31, 072710 (2024)

<https://doi.org/10.1063/5.0211691>



### Articles You May Be Interested In

Stopping power of high-density alpha-particle clusters in partially degenerated deuterium–tritium fuels

*Phys. Plasmas* (July 2023)

Mitigation of hot-electron preheat from the two-plasmon-decay instability using silicon-doped plastic shells in direct-drive implosions on OMEGA

*Phys. Plasmas* (November 2024)

Enhanced laser-target energy coupling through counter-propagating lasers: Insights from electron recirculation

*Phys. Plasmas* (November 2024)



Physics of Plasmas

Special Topics Open  
for Submissions

[Learn More](#)

# Non-equilibrium and self-organization evolution in hot-spot ignition processes

Cite as: Phys. Plasmas **31**, 072710 (2024); doi: [10.1063/5.0211691](https://doi.org/10.1063/5.0211691)

Submitted: 1 April 2024 · Accepted: 5 July 2024 ·

Published Online: 26 July 2024



View Online



Export Citation



CrossMark

X.-Y. Fu,<sup>1,2</sup> Z.-Y. Guo,<sup>1,2</sup> Q.-H. Wang,<sup>1,2</sup> R.-C. Wang,<sup>1,2</sup> D. Wu,<sup>1,2,a)</sup> and J. Zhang<sup>1,2,3,a)</sup>

## AFFILIATIONS

<sup>1</sup>Key Laboratory for Laser Plasmas and Department of Physics and Astronomy, Collaborative Innovation Center of IFSA (CICTFSA), Shanghai Jiao Tong University, Shanghai 200240, People's Republic of China

<sup>2</sup>Zhiyuan College, Shanghai Jiao Tong University, Shanghai 200240, People's Republic of China

<sup>3</sup>Institute of Physics, Chinese Academy of Sciences, Beijing 100190, People's Republic of China

<sup>a)</sup>Authors to whom correspondence should be addressed: [dwu.phys@sjtu.edu.cn](mailto:dwu.phys@sjtu.edu.cn) and [jzhang1@sjtu.edu.cn](mailto:jzhang1@sjtu.edu.cn)

## ABSTRACT

In inertial confinement fusion systems, achieving ignition can be pursued through two main approaches—central hot-spot ignition and fast ignition. Due to disparate formation mechanisms in these methods, the initial temperatures of electrons and ions in the hot spot often differ, highlighting the limitations of equilibrium theoretical models in accurately capturing the ignition conditions and evolution of the hot spot. In this work, we present a non-equilibrium model and extended this model to both isobaric and isochoric scenarios, characterized by varying hot-spot densities, temperatures, and expansion velocities. In both cases, a spontaneous self-organization evolution was observed, manifesting as the bifurcation of ion and electron temperatures. Notably, the ion temperature is particularly prominent during the ignition process. This inevitability can be traced to the preponderant deposition rates of alpha-particles into D-T ions and the decreasing rate of energy exchange between electrons and D-T ions at elevated temperatures. The inherent structure, characterized by higher ion temperature and lower electron temperature during ignition, directly contributes to the augmentation of D-T reactions and mitigates energy losses through electron conduction and bremsstrahlung, thereby naturally facilitating nuclear fusions.

© 2024 Author(s). All article content, except where otherwise noted, is licensed under a Creative Commons Attribution (CC BY) license (<https://creativecommons.org/licenses/by/4.0/>). <https://doi.org/10.1063/5.0211691>

## I. INTRODUCTION

Inertial confinement fusion encompasses several approaches to ignition, including central hot spot ignition,<sup>1</sup> volume ignition, such as double shell, and fast ignition capsules. Each approach involves distinct processes for the formation of a hot, burning plasma. In central hot-spot ignition, for instance, pulse shaping of the laser is crucial to selectively compress and heat a portion of the D-T fuel to ignition conditions. In this ignition method, which is powered by x-rays or lasers, the D-T gas, along with the surrounding high density D-T fuel, is compressed inward, leading to the formation of a high-temperature hot spot at the core of the fuel. Conventionally, the hot spot achieved through this design maintains nearly constant pressure compared to the surrounding cold fuels.<sup>2</sup> During the implosion process, the majority of the shock wave energy is deposited into ions, resulting in elevated ion temperatures, as experimentally verified.<sup>3</sup> In contrast, the fast ignition scheme separates the compression and hot-spot formation processes.<sup>4–6</sup> During the compression, the density remains uniform,

necessitating the employment of an isochoric model.<sup>7–9</sup> After the compression process, a beam of fast electrons is injected and deposited, resulting in the formation of a localized hot spot with an electron temperature significantly higher than that of the ions.<sup>6</sup>

The central hot-spot design has remained the prevailing strategy and has attained several milestones in recent years, e.g., burning plasma state,<sup>10</sup> ignition,<sup>11</sup> and “scientific breakeven.”<sup>1</sup> Despite this achievement, there are still unresolved facets of new physics within the burning plasmas and ignition processes, as detailed in Refs. 10, 12, and 13. These include kinetic effects and the energy transfer mechanisms of  $\alpha$ -particles during the self-burning processes, as evidenced in Ref. 14.

Concerning the unresolved ignition queries, previous theoretical efforts have primarily resorted to a simplified equilibrium model.<sup>15–19</sup> For the sake of simplicity, it has become commonplace to assume nearly identical ion and electron temperatures throughout the ignition process.<sup>20,21</sup> However, this approach overlooks the likelihood of non-equilibrium ion and electron temperatures. We hypothesize that, at

high temperatures, the equilibrium condition might be disrupted due to different heating mechanisms acting on ions and electrons, resulting in distinct evolution.

In Fan's work, the ion-electron non-equilibrium ignition was theoretically studied through the introduction of a two-temperature model.<sup>22</sup> They consider separate thermal equilibrium of ions and electrons at temperatures  $T_i$  and  $T_e$  ( $T_i \neq T_e$ ). Consequently, these two components evolve independently with energy exchange between them due to ion-electron collisions. According to their findings, an initially higher hot spot ion temperature compared to electrons enhances nuclear reactions and reduces energy loss of electron conduction and bremsstrahlung, thereby facilitating ignition. Building upon their model, we further develop an isochoric model for fast ignition, depict the ignition condition in different cases, and provide a detailed analysis of different heating stages during both hot-spot ignition and fast ignition processes. In the context of fast ignition, the disparity between ion and electron temperatures exerts a significant influence on the heating process due to extreme density, offering valuable insights for optimizing the hot-spot formation process. Additionally, disparate deposition rates of alpha-particle heating of ions and electrons lead to the bifurcated evolution of ion and electron temperatures, ultimately and naturally benefiting ignition.

The organization of this paper is as follows. In Sec. II, we introduce the equations that form the basis of our non-equilibrium model. Subsequently, Sec. III offers an overview of the data sources employed and presents our simulation outcomes for both the isobaric and isochoric models. Furthermore, Sec. IV delves into a theoretical analysis of the distinct temporal stages observed in the heating process. Finally, Sec. V concludes the paper by summarizing our key findings and discussing their implications.

## II. NON-EQUILIBRIUM MODEL

The hot spot, characterized by its radius  $R_h$  and total density  $\rho_h$ , can be simplified as comprising two components: D-T ions and electrons. Ion temperatures and pressures are denoted as  $T_i$  and  $P_i$ , respectively, and electron temperatures and pressures are denoted as  $T_e$  and  $P_e$ , respectively; then, we define the hot-spot equilibrium temperature as  $T_h \equiv (T_i + T_e)/2$  and introduce a non-equilibrium factor,  $f = T_i/T_h$ .

During ignition, the alpha particles produced by D-T reactions, primarily concerned with the ion temperature  $T_i$ , deposit energy into the hot spot at a total power of  $W_\alpha = A_\alpha \rho_h^2 \langle \sigma v \rangle f_\alpha$  in unit of W/m<sup>3</sup> (note that all units of energy discussed in this work follow the International System of Units and are W/m<sup>3</sup>), with  $A_\alpha = 8 \times 10^{40}$  erg/g<sup>2</sup>. Here,  $\langle \sigma v \rangle$  is the cross section of D-T fusion, expressed as a function of  $T_i$ .<sup>5</sup> The deposition rate of  $\alpha$  in hot spots  $f_\alpha$  has a form of

$$f_\alpha = \begin{cases} (3/2)\tau_\alpha - (4/5)\tau_\alpha^2, & \tau_\alpha \leq 1/2, \\ 1 - (1/4)\tau_\alpha^{-1} + (1/160)\tau_\alpha^{-3}, & \tau_\alpha \geq 1/2, \end{cases} \quad (1)$$

where  $\tau_\alpha \simeq 9 \times \ln \Lambda \rho_h R_h / T_h^{3/2}$ . This energy deposition heats the ions and electrons in the hot spot by fractions of  $f_{\alpha i} = T_e/(32 + T_e)$  and  $f_{\alpha e} = 1 - f_{\alpha i}$ , respectively, where  $T_e$  is given in kilo-electron volt.<sup>23</sup> The energy losses in the system occur through electron thermal conduction with the surrounding main fuel, given by

$W_e = 3A_e T_e^{7/2} / R_h^2 / \ln \Lambda$  with  $A_e = 9.5 \times 10^{19}$  erg s<sup>-1</sup> cm<sup>-1</sup> keV<sup>-7/2</sup>, and through electron bremsstrahlung  $W_r = A_r \rho_h^2 T_e^{1/2}$  with  $A_r = 3.05 \times 10^{23}$  erg cm<sup>3</sup> g<sup>-2</sup> s<sup>-1</sup> keV<sup>-1/2</sup>. The Coulomb logarithm  $\ln \Lambda$  can be expressed as  $0.5 \times \ln [1 + (b_{\min}/b_{\max})^2]$ ,<sup>24</sup> where  $b_{\min}$  is the maximum between the classical impact parameter and the De Broglie wavelength, and  $b_{\max}$  is the Debye length. Additionally, the expansion of the ions and electrons within the hot spot, together with speed  $u_h$ , contributes to energy loss with powers of  $W_{m,i} = 3P_i u_h / R_h$  and  $W_{m,e} = 3P_e u_h / R_h$ , respectively. Furthermore, energy exchange between ions and electrons occurs through collisions, contributing to a power of  $W_{ie} = A_{\omega,ei} \rho_h^2 \ln \Lambda (T_i - T_e) / T_e^{3/2}$ , where  $A_{\omega,ei} = 5.6 \times 10^{14}$  kJ cm<sup>3</sup> g<sup>-2</sup> s<sup>-1</sup> keV<sup>1/2</sup>.

The temporal evolution for the temperatures of ion and electron energies, accounting for both the energy gains and losses in the hot spot, is expressed as follows:<sup>22</sup>

$$C_{V,i} \rho_i \frac{dT_i}{dt} = W_\alpha f_{\alpha i} - W_{ie} - W_{m,i}, \quad (2)$$

$$C_{V,e} \rho_e \frac{dT_e}{dt} = W_\alpha f_{\alpha e} + W_{ie} - W_{m,e} - W_r - W_e, \quad (3)$$

where  $C_{V,i}$  and  $C_{V,e}$  are the specific heat of ions and electrons, respectively, and  $\rho_i$  and  $\rho_e$  are the density of ions and electrons, respectively.

We account for energy spreading outside the hot spot by including the electron bremsstrahlung power  $W_r$  and electron thermal conduction  $W_e$ . The latter contributes to main fuel ablation, ultimately increasing the hot-spot mass, which is expressed as<sup>20,21,25</sup>

$$\frac{d\rho_h V_h}{dt} = \frac{[W_r + W_e + W_\alpha(1 - f_\alpha)/f_\alpha] V_h}{C_{v,i} T_i + C_{v,e} T_e}. \quad (4)$$

Our primary interest lies in the density variation; therefore, we formulate the contribution of volume  $V_h$  and rewrite Eq. (4) as

$$\frac{d\rho_h}{dt} = \frac{W_r + W_e + W_\alpha(1 - f_\alpha)/f_\alpha}{C_{v,i} T_i + C_{v,e} T_e} - \frac{4\pi R_h^2 \rho_h u_h}{V_h}, \quad (5)$$

considering the hot-spot expansion rate given by

$$\frac{dR_h}{dt} = u_h. \quad (6)$$

In our research, significant attention is focused on the moment of stagnation, which lies between the end of compression and the decomposition of the hot spot. This transient yet pivotal moment exhibits distinct behaviors in response to the different ignition approaches. In the case of central hot-spot ignition, the hot spot follows the isobaric description, where the hot-spot pressure approximates that of the surrounding cold fuel, resulting in minimal alterations to its radius.<sup>21,26</sup> Conversely, the fast ignition scheme features a hot-spot density that closely mirrors the cold fuel, utilizing the isochoric model.<sup>7</sup> Consequently, the hot spots expand due to pressure differentials. The intricate relationship between these models is graphically represented in Fig. 1. The respective expansion rates for these models are mathematically described in Ref. 5,

$$u_h = \begin{cases} \sim 0, & \text{Isobaric model,} \\ \sim \left( \frac{3}{4} \Gamma_B T_h \frac{\rho_h}{\rho_c} \right)^{1/2}, & \text{Isochoric model,} \end{cases} \quad (7)$$

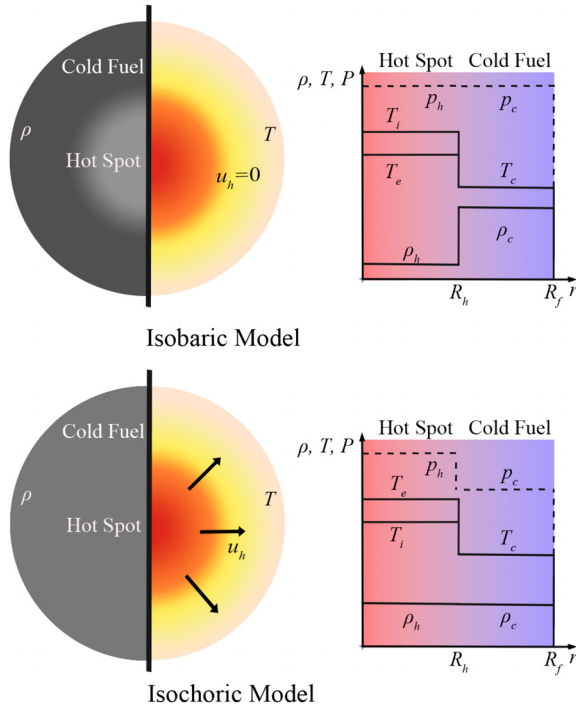


FIG. 1. Schematic description of isobaric and isochoric hot-spot ignition models.

where  $\Gamma_B$  is related to the Boltzmann constant, for D-T fuel,  $\Gamma_B = 4k_B/(2m_e + 5m_p) = 7.66 \times 10^{14} \text{ erg/(g keV)}$ , and  $\rho_h$  and  $\rho_c$  are, respectively, the density of the hot spot and the main fuel. Due to the physical nature of these four equations, our model can only be applied during the stagnation phase, which is the time period when compression is essentially completed, but the burning wave has not yet disintegrated the hot spot. Therefore, our assumption of no expansion in the isochoric model is justified.

By solving the aforementioned set of four differential equations, we obtain valuable insights into the ignition processes, which are elucidated in Sec. III.

### III. NUMERICAL RESULTS

In Sec. II, we have presented a set of differential equations for temporal evolution of physical quantities, using the basic forward Euler method. In this section, this set of equations is numerically solved and displayed. In Table I, the initial parameters are displayed, and especially, the areal density is kept the same in both models for a consistent comparison between them.

TABLE I. Numerical analyses with different initial conditions, including the radius, density and temperature of the hot spot, for both isobaric and isochoric models.

Scheme	$R_h$ ( $\mu\text{m}$ )	$\rho_h$ ( $\text{g/cm}^3$ )	$T_h$ (keV)	$\rho_c$ ( $\text{g/cm}^3$ )
Isobaric model	100	100	8	1000
Isochoric model	100	300	8	300

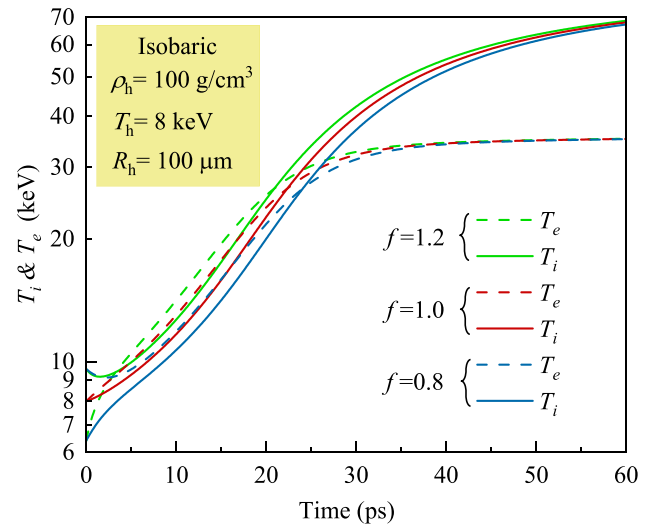


FIG. 2. In the isobaric model, with areal density of  $\rho_h R_h = 10 \text{ g/cm}^2$ , the ion and electron temperature rise as a function of time for different initial non-equilibrium factors  $f = 0.8, 1$  and  $1.2$ . These two temperatures would finally become bifurcated and reach saturated values.

To investigate the non-equilibrium dynamics comprehensively, we conduct numerical analyses with initial states of various conditions for both isochoric and isobaric models. Our study involves analyzing the temporal evolution of the electron temperature and ion temperature. Additionally, we explore the distribution of initial values leading to successful ignition within the phase space (areal density and temperature) over a finite time. These analyses aim to delineate the ignition thresholds associated with distinct equilibrium factors and models.

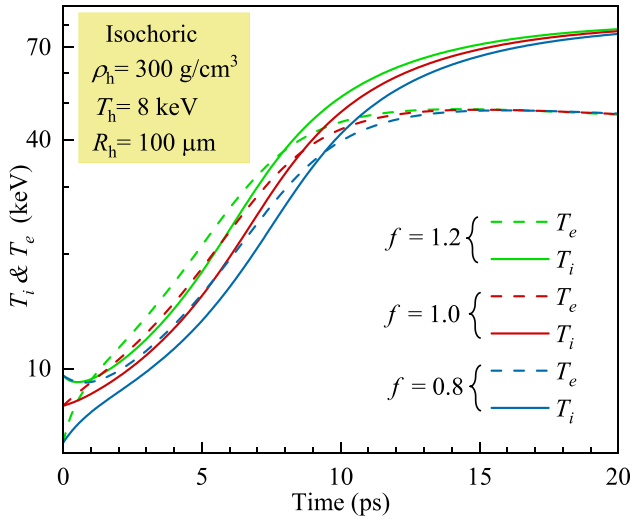
#### A. Isobaric model

Figure 2 shows the temperature evolution for the isobaric model. From this evolution curve, we find that the electrons and ions first undergo energy exchange with each other, similar to a relaxation process.<sup>27</sup> Then, the temperature of the two species rises steadily until it reaches a certain value where separation occurs, which will be discussed in detail in Sec. IV. During the entire process, a remarkable phenomenon occurs: after reaching a specific value, the temperatures of ions and electrons spontaneously diverge, ultimately reaching their saturated states. This heating process can be therefore broadly categorized into four distinct stages, and in the following, we will elucidate each of them.

Under the influence of the non-equilibrium factor, we can find that the ignition is more easier to achieve under same initial conditions when the non-equilibrium factor is high, which means the initial temperature of ions is higher than that of electrons.

#### B. Isochoric model

Figure 3 reveals that the temporal evolution of temperatures for the isochoric model is quite similar to that of the isobaric model. The influence of the non-equilibrium factor remains consistent with that observed in the isobaric model. Notably, the temperature of ions plays a pivotal role in the heating process. However, there still exist two



**FIG. 3.** In the isochoric model with an areal density  $\rho_h R_h = 10 \text{ g/cm}^2$ , the ion and electron temperature rise with time at different initial non-equilibrium factors  $f = 0.8, 1, \text{ and } 1.2$ . These two temperatures will become bifurcated and eventually decrease due to expansion.

main differences. First, if the time duration is significantly extended, the temperature of both ions and electrons will decrease as a result of the expansion of the hot spot, and this trend is more significant in the isochoric model. Second, by comparing the first 5 ps in Figs. 2 and 3, we observe significant differences in between the isobaric and isochoric models. Notably, in the isochoric model, DT hot spot heats up considerably faster than the isobaric model, resulting in a much higher peak temperature.

### C. Ignition condition

The ignition threshold curve in Fig. 4 establishes the boundaries within the initial phase space (areal density and temperature) that permit successful ignition within a finite time span. In our simulations, a main criterion on the second derivative of temperature ( $d^2T/dt^2 > 0$ ) has been applied to determine the success of the ignition for a given set of initial conditions.<sup>11,28</sup> It is worth mentioning that a stronger ignition condition is used in the literature.<sup>29</sup> This does not change our conclusions, but would change the location of the ignition curves to higher temperature and areal density. Specifically, an excessively low areal density is precluded as it hinders electron heat conduction at elevated temperatures, as discussed in Ref. 30. Conversely, a high areal density enables the temperature to approach closely the critical value of 4.3 keV, which is essential for self-heating. In general, our ignition threshold curve shares the same signatures with other detailed analysis<sup>21,29</sup> and gives a wider allowed area for ignition at high temperatures. We further explore the effects of non-equilibrium factor  $f$ . With larger  $f$  applied, the ignition area will be expanded.

In comparison, the isobaric model exhibits less stringent ignition requirements than the isochoric model, as shown in Fig. 4. Regardless of the model chosen, an increase in the non-equilibrium factor plays a pivotal role in expanding the ignition area. This underscores the positive impact of enhancing the non-equilibrium factor, which effectively lowers ignition thresholds.

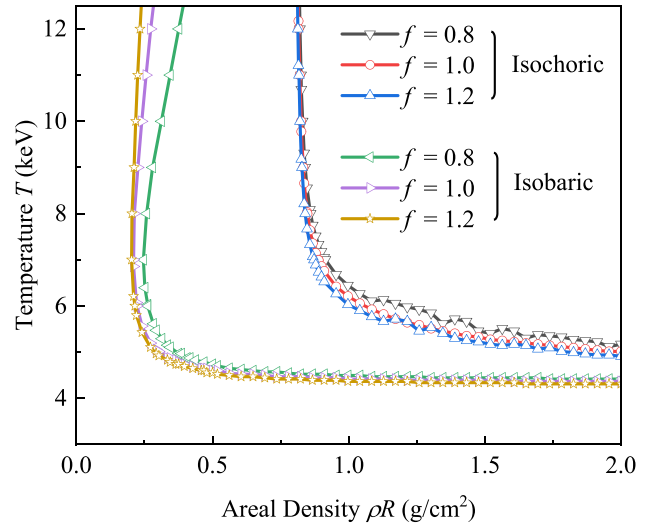


**FIG. 4.** The ignition condition for both isobaric and isochoric models. When the initial condition of the hot spot is above the curve, the ignition would take place.

### IV. ANALYSIS OF IGNITION EVOLUTION

In the ignition process, depicted in Fig. 5, intriguing phenomena emerge, indicating that the heating process can be segmented into four distinct stages: thermal equilibrium (stage A), co-heating (stage B), bifurcated heating (stage C), and attaining saturated temperatures (stage D). We aim to delve into each of these processes and provide a theoretical analysis. Figure 5 also illustrates the power per unit volume throughout the ignition process. Notably, the expansion work in the isobaric model is ignored. The exchange energy between ions and electrons, however, is influenced by both the temperature of the ions and electrons, necessitating the utilization of an absolute value for this particular energy component.

Our focus will primarily be on analyzing the isobaric model, while the ignition process is also shown in Fig. 6. As mentioned in Sec. III B, the isochoric model exhibits similarities to the isobaric model in terms of its physical characteristics. However, a key distinction lies in the final process, which is influenced by the dominance of expansion power  $W_m$ .

#### A. Reaching a dynamic equilibrium

At the beginning, the average temperature of ions and electrons does not increase significantly, but the temperature difference gradually decreases, as presented in the stage A of Fig. 5. We therefore subtract Eq. (2) from Eq. (3), to derive the temperature differences between ions and electrons. With relations  $C_{V,i} = 3k_B/(2m_i)$ ,  $C_{V,e} = 3k_B/(2m_e)$ , and  $C_{V,i}\rho_i = C_{V,e}\rho_e$ , we can get

$$C_{V,i}\rho_i \frac{d\Delta T}{dt} = W_\alpha \frac{T_e - 32 \text{ keV}}{T_e + 32 \text{ keV}} - 2W_{ie} - W_{m,i} + W_{m,e} + W_r + W_e, \quad (8)$$

where  $\Delta T = T_i - T_e$ . In the isobaric model,  $u_h \sim 0$ , meaning that the expansion of ions and electrons does not contribute to energy loss. Consequently, both  $W_{m,i}$  and  $W_{m,e}$  are zero. At the beginning of the



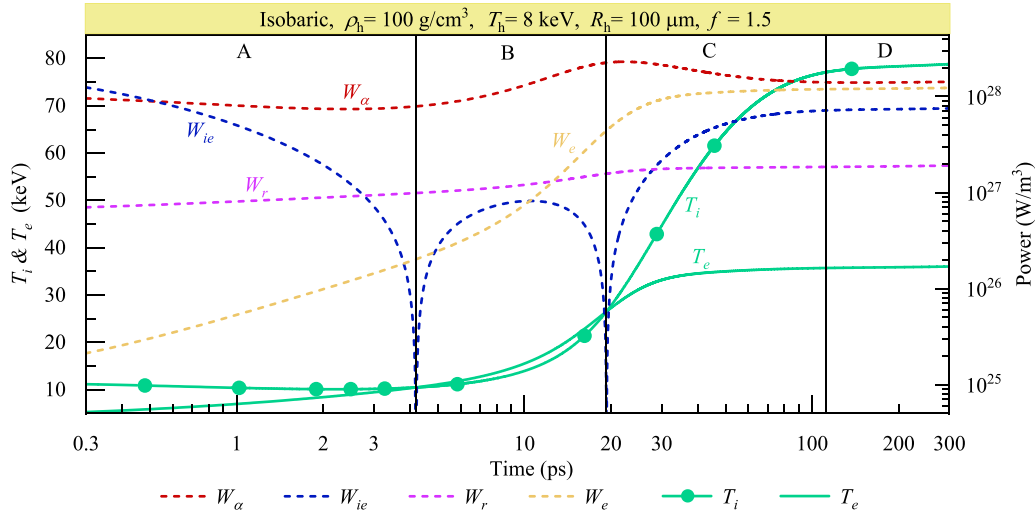


**FIG. 5.** The ignition process for an isobaric model, with  $T_i$ ,  $T_e$ ,  $W_\alpha$ ,  $W_{ie}$ ,  $W_r$ , and  $W_e$  evolving as a function of time. It's important to note that since our differential equation only holds at the stagnation moments, the curve after 100 ps is just an esthetic extension.

ignition process, when the electron and ion temperature are sufficiently low,  $W_\alpha \propto \langle \sigma v \rangle$ , which strongly depends on the ion temperature,<sup>5</sup>  $W_r \propto T_e^{1/2}$  and  $W_e \propto T_e^{7/2}$ . Instead,  $W_{ie} \propto \Delta T \cdot T_e^{-3/2}$ , which means that at low temperatures, energy exchange between the ions and electrons dominates, as demonstrated in Fig. 5. Also, due to the  $\Delta T$  dependence and the large coefficient  $A_{\omega,ei}$  in the ion-electron energy exchange power  $W_{ie}$ ,  $W_{ie}$  will dominate for a while before the temperature reaches a high level. Consequently, the temperature difference between ions and electrons starts to shrink, reaching a

dynamic equilibrium. However, when the initial temperature difference is minimal (i.e.,  $f$  is close to 1), the process becomes less distinct, as it can be interpreted as having reached a state of dynamic equilibrium.

In comparison, we choose  $f = 0.8 < 1$  in the isochoric case shown in Fig. 6 and find the stage A disappears. The much denser hot spot in the isochoric case leads to a dominating  $\alpha$ -particle heating, thus preventing ions and electrons to reach a thermal equilibrium and making stage A invisible.

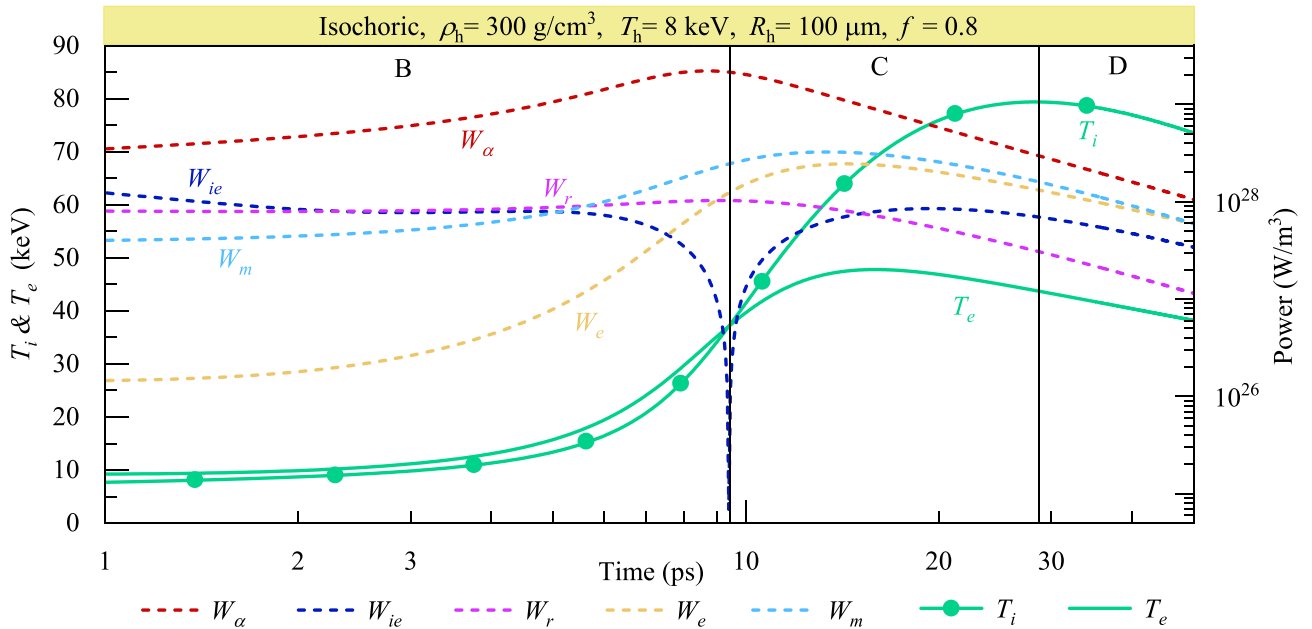


**FIG. 6.** The ignition process for an isochoric model, with  $T_i$ ,  $T_e$ ,  $W_\alpha$ ,  $W_{ie}$ ,  $W_r$ ,  $W_e$ , and  $W_m = W_{m,i} + W_{m,e}$  evolving as a function of time.

## B. Co-heating as an equilibrium model

As the ion and electron temperatures converge, they can be heated simultaneously under the influence of an increasing  $\alpha$ -particle heating power  $W_\alpha$ , as shown in stage B of Fig. 5. During this process, the ion-electron collisions maintain  $T_e \approx T_i$  dynamically, by balancing the terms, e.g.,  $W_\alpha(f_{xi} - f_{xe})$ ,  $2W_{ie}$ ,  $W_r$ , and  $W_e$ , in Eq. (8). During the B stage depicted in Fig. 5, the  $\alpha$ -heating power significantly surpasses other energy loss powers, resulting in a co-heating process. However, as the electron temperature  $T_e$  rises, the electron conduction power experiences a remarkable increase due to its  $T_e^{7/2}$  dependence. When the electron temperature approaches approximately  $\sim 32$  eV,  $W_\alpha(f_{xi} - f_{xe})$  undergoes a sign change, indicating that the difference between the  $\alpha$ -particle heating contributions to the ion and electron temperatures is poised to reverse. These observations suggest that the balance maintained by the ion-electron collisions in Eq. (8) may be disrupted.

## C. Bifurcated heating

In stage C depicted in Fig. 5, the evolution of the ion and electron temperatures,  $T_i$  and  $T_e$ , diverges significantly. This divergence can be attributed to the weakened ion-electron energy exchange power,  $W_{ie} \propto \Delta T / (T_e)^{3/2}$ , at high electron temperatures, as well as the differing energy loss and heating mechanisms between ions and electrons.

The heating effect on electron temperature is significantly suppressed, while ion temperature heating remains robust during stage C. For electrons, the significant enhancement in electron conduction loss,  $W_e \propto T_e^{7/2} \sim 10^{28}$ , strongly constrains the growth of the electron temperature,  $T_e$ . As evident in Eq. (3), the  $\alpha$ -particle heating power,  $W_\alpha \sim 10^{28}$ , is effectively suppressed by  $W_e$ . Furthermore, the electron temperature  $T_e$  increases at a rate proportional to  $W_{ie} \propto \Delta T / (T_e)^{3/2}$ , which is insufficient to keep up with the ion temperature. This trend is clearly illustrated in Fig. 5. Consequently, the electron temperature exhibits a slow growth ( $\Delta T_e \sim 5$  keV) that can be disregarded, resulting in a gradual increase in  $W_e$  toward a maximum value. Meanwhile,  $f_{xi}$  and  $f_{xe}$  remain virtually unchanged, and  $W_{ie}$  exhibits a nearly linear increase with  $\propto \Delta T$ . For ions, we examine Eq. (2) and discover that they lack a significant energy loss mechanism besides transferring energy to electrons through collisions. Given the slow but steady increase in the relatively low energy exchange power  $W_{ie}$ , the heating effect from  $\alpha$ -particles, represented by  $W_{xi} = W_\alpha f_{xi}$ , dominates the ion temperature growth, resulting in a significant increase. Consequently,  $T_i$  rises extremely rapidly, eventually pushing the ion-electron energy exchange power  $W_{ie}$  to a notably high level. Meanwhile, the decreasing value of  $f_x$  is accompanied by a weakening of  $W_\alpha$ . To conclude, we refer to Eq. (8), which reveals that the difference in  $\alpha$ -particle heating,  $W_\alpha(f_{xi} - f_{xe}) \sim 10^{27}$  W/m<sup>3</sup>, is significant. Additionally, the ion-electron energy exchange power, which is slowly increasing, contributes  $2W_{ie} \sim 10^{26-27}$  W/m<sup>3</sup> to the overall heating process. However, the dominant factor is the electron conduction loss, estimated to be  $W_e \sim 10^{28}$  W/m<sup>3</sup>. Consequently, the ion and electron temperatures diverge significantly as they evolve.

## D. Reaching saturated temperatures

During the stage D depicted in Fig. 5, a saturation phenomenon becomes evident in both ion and electron temperatures. We have mentioned the slowly growing electron temperature  $T_e$ ,

electron conduction loss  $W_e$ , the increasing ion temperature  $T_i$ , ion-electron energy exchange  $W_{ie}$ , and the decreasing  $\alpha$ -particle heating  $W_\alpha$  in stage C. With an increasing temperature gradient, the energy exchange  $W_{ie}$  between ions and electrons significantly increases. This enhancement allows the energy exchange to be comparable with both the electron thermal conduction loss  $W_e$  and the  $\alpha$ -particle heating  $W_\alpha f_{xe}$ ; ultimately, a balance is achieved between the energy loss and gain for electrons. Subsequently, the electron temperature nearly attains a state of saturation. Later, with the increase in  $T_i$ , the  $\alpha$ -particle heating power decreases, while the ion-electron energy exchange  $W_{ie}$  continues to adjust, maintaining the saturation of the electron temperature  $T_e$ . Eventually, the heating power from  $\alpha$ -particles, represented by  $W_\alpha$ ,  $W_{xi}$  will decline to a certain low level, reaching a balance with the ion-electron conduction  $W_{ie}$  as expressed in Eq. (2). This balance contributes to the saturation of the ion temperature  $T_i$ .

Note that our model is applicable around the stagnation phase, which typically lasts for tens of picoseconds. However, in Figs. 5 and 6, results well beyond the capabilities of our model are displayed for the intuitiveness of the image. This does not affect our conclusions, as the co-heating and bifurcated heating phenomena occur in the first few tens of picoseconds.

The intricate internal plasma environment poses significant non-linear constraints, stemming from the diverse energy gain and loss mechanisms at play. However, the ion-electron energy exchange, functioning as a self-regulating quantity, dynamically adjusts in response to the varying energy gain and loss mechanisms of ions and electrons, ultimately leading to the saturation phenomenon. This phenomenon serves as a vivid illustration of the complex non-linear constraints inherent in fusion plasmas. Furthermore, our results underscore a non-isothermal phenomenon that plays a pivotal role in enhancing the efficient burning of hot spots. Notably, the primary energy loss mechanism in hot spots is closely linked to the electron temperature, whereas the fusion heating mechanism exhibits a positive correlation with ion temperature. This dynamic imbalance gives rise to a non-equilibrium hot-spot model, which emerges as an inevitable outcome and represents one of our most valuable predictions.

## V. CONCLUSION AND DISCUSSIONS

In our research, we derive a non-equilibrium ion-electron model, extending it to consider both isobaric and isochoric conditions. These conditions exhibit variations in the densities, temperatures, and expansion velocities of the hot spot. Our results reveal intriguing self-organization phenomena in ion and electron temperatures during the ignition process. Specifically, we find that ion temperature dominates over the electron temperature in this process. This phenomenon arises due to the significant heating effect caused by alpha particles, as well as the distinct deposition rates of alpha particle heating at high temperatures. Additionally, the reduced rate of energy exchange between electrons and D-T ions contributes to the observed bifurcation. During ignition, the inherent structure of higher ion temperature and lower electron temperature directly promotes the enhancement of the D-T reaction and reduces energy loss through electron conduction. Consequently, our ion-electron non-equilibrium model holds promise for improving inertial fusion ignition performed at current mega-joule laser facilities.

## ACKNOWLEDGMENTS

This work is supported by the Strategic Priority Research Program of Chinese Academy of Sciences (Grant Nos. XDA25010100 and XDA250050500), National Natural Science Foundation of China (Grant No. 12075204), and Shanghai Municipal Science and Technology Key Project (No. 22JC1401500). Dong Wu thanks the sponsorship from Yangyang Development Fund. The junior undergraduate students, X.-Y. Fu, Z.-Y. Guo, Q.-H. Wang, and R.-C. Wang, all contributed equally to this work. The authors would like to thank Dr. Zekun Xu for useful discussions.

## AUTHOR DECLARATIONS

## Conflict of Interest

The authors have no conflicts to disclose.

## Author Contributions

**X. Y. Fu:** Conceptualization (equal); Formal analysis (equal); Investigation (equal); Validation (equal); Writing – original draft (equal); Writing – review & editing (equal). **Z. Y. Guo:** Conceptualization (equal); Data curation (equal); Formal analysis (equal); Investigation (equal); Methodology (equal); Software (supporting); Validation (equal); Writing – original draft (equal); Writing – review & editing (equal). **Q. H. Wang:** Conceptualization (equal); Data curation (equal); Formal analysis (equal); Investigation (equal); Methodology (equal); Software (equal); Validation (equal); Writing – original draft (equal); Writing – review & editing (equal). **R.-C. Wang:** Conceptualization (equal); Investigation (equal); Validation (equal); Writing – original draft (equal); Writing – review & editing (equal). **D. Wu:** Conceptualization (equal); Formal analysis (equal); Funding acquisition (equal); Investigation (lead); Project administration (lead); Supervision (lead); Writing – review & editing (lead). **J. Zhang:** Conceptualization (equal); Funding acquisition (equal); Investigation (equal); Project administration (equal); Supervision (equal).

## DATA AVAILABILITY

The data that support the findings of this study are available from the corresponding author upon reasonable request.

## REFERENCES

- <sup>1</sup>R. Acree, H. Abu-Shawareb, P. Adams, J. Adams, B. Addis, R. Aden, P. Adrian, B. B. Afeyan, M. Aggleton, L. Aghaian *et al.*, *Phys. Rev. Lett.* **132**, 065102 (2024).
- <sup>2</sup>P. Clavin, *Combust. Flame* **175**, 80 (2017).
- <sup>3</sup>J. R. Rygg, J. A. Frenje, C. K. Li, F. H. Séguin, R. D. Petrasso, D. D. Meyerhofer, and C. Stoeckl, *Phys. Rev. E* **80**, 026403 (2009).
- <sup>4</sup>M. Tabak, D. Hinkel, S. Atzeni, E. M. Campbell, and K. Tanaka, *Fusion Sci. Technol.* **49**, 254 (2006).
- <sup>5</sup>S. Atzeni, in *Laser-Plasma Interactions and Applications*, edited by P. McKenna, D. Neely, R. Bingham, and D. Jaroszynski (Springer International Publishing, 2013), pp. 243–277.
- <sup>6</sup>S. A. Ghasemi, A. H. Farahbod, and S. Sobhanian, *AIP Adv.* **4**, 077130 (2014).
- <sup>7</sup>Z. Xu, F. Wu, B. Jiang, S. Kawata, and J. Zhang, *Nucl. Fusion* **63**, 126062 (2023).
- <sup>8</sup>D. S. Clark and M. Tabak, *Nucl. Fusion* **47**, 1147 (2007).
- <sup>9</sup>A. H. Farahbod, S. A. Ghasemi, M. J. Jafari, S. Rezaei, and S. Sobhanian, *Eur. Phys. J. D* **68**, 314 (2014).

- <sup>10</sup>A. B. Zylstra, O. A. Hurricane, D. A. Callahan, A. L. Kritcher, J. E. Ralph, H. F. Robey, J. S. Ross, C. V. Young, K. L. Baker, D. T. Casey, T. Döppner, L. Divol, M. Hohenberger, S. Le Pape, A. Pak, P. K. Patel, R. Tommasini, S. J. Ali, P. A. Amendt, L. J. Atherton, B. Bachmann, D. Bailey, L. R. Benedetti, L. Berzak Hopkins, R. Betti, S. D. Bhandarkar, J. Biener, R. M. Bionta, N. W. Birge, E. J. Bond, D. K. Bradley, T. Braun, T. M. Briggs, M. W. Bruhn, P. M. Celliers, B. Chang, T. Chapman, H. Chen, C. Choate, A. R. Christopherson, D. S. Clark, J. W. Crippen, E. L. Dewald, T. R. Dittrich, M. J. Edwards, W. A. Farmer, J. E. Field, D. Fittinghoff, J. Frenje, J. Gaffney, M. Gatu Johnson, S. H. Glenzer, G. P. Grim, S. Haan, K. D. Hahn, G. N. Hall, B. A. Hammel, J. Harte, E. Hartouni, J. E. Heebner, V. J. Hernandez, H. Herrmann, M. C. Herrmann, D. E. Hinkel, D. D. Ho, J. P. Holder, W. W. Hsing, H. Huang, K. D. Humbird, N. Izumi, L. C. Jarrott, J. Jeet, O. Jones, G. D. Kerbel, S. M. Kerr, S. F. Khan, J. Kilkenny, Y. Kim, H. Geppert Kleinrath, V. Geppert Kleinrath, C. Kong, J. M. Koning, J. J. Kroll, M. K. G. Kruse, B. Kustowski, O. L. Landen, S. Langer, D. Larson, N. C. Lemos, J. D. Lindl, T. Ma, M. J. MacDonald, B. J. MacGowan, J. Mackinnon, S. A. MacLaren, A. G. MacPhee, M. M. Marinak, D. A. Mariscal, E. V. Marley, L. Masse, K. Meaney, N. B. Meezan, P. A. Michel, M. Millot, J. L. Milovich, J. D. Moody, A. S. Moore, J. W. Morton, T. Murphy, K. Newman, J.-M. G. D. Nicola, A. Nikroo, R. Nora, M. V. Patel, L. J. Pelz, J. L. Peterson, Y. Ping, B. B. Pollock, M. Ratledge, N. G. Rice, H. Rinderknecht, M. Rosen, M. S. Rubery, J. D. Salmonson, J. Sater, S. Schiaffino, D. J. Schlossberg, M. B. Schneider, C. R. Schroeder, H. A. Scott, S. M. Sepke, K. Sequoia, M. W. Sherlock, S. Shin, V. A. Smalyuk, B. K. Spears, P. T. Springer, M. Stadermann, S. Stoupin, D. J. Strozzi, L. J. Suter, C. A. Thomas, R. P. J. Town, E. R. Tubman, C. Troselle, P. L. Volegov, C. R. Weber, K. Widmann, C. Wild, C. H. Wilde, B. M. Van Wouterghem, D. T. Woods, B. N. Woodworth, M. Yamaguchi, S. T. Yang, and G. B. Zimmerman, *Nature* **601**, 542 (2022).
- <sup>11</sup>R. Acree, H. Abu-Shawareb, P. Adams, J. Adams, B. Addis, R. Aden, P. Adrian, B. B. Afeyan, M. Aggleton, L. Aghaian *et al.*, *Phys. Rev. Lett.* **129**, 075001 (2022).
- <sup>12</sup>O. A. Hurricane, D. A. Callahan, D. T. Casey, P. M. Celliers, C. Cerjan, E. L. Dewald, T. R. Dittrich, T. Döppner, D. E. Hinkel, L. F. B. Hopkins, J. L. Kline, S. Le Pape, T. Ma, A. G. MacPhee, J. L. Milovich, A. Pak, H.-S. Park, P. K. Patel, B. A. Remington, J. D. Salmonson, P. T. Springer, and R. Tommasini, *Nature* **506**, 343 (2014).
- <sup>13</sup>J. Lindl, O. Landen, J. Edwards, E. Moses, and NIC Team, *Phys. Plasmas* **21**, 020501 (2014).
- <sup>14</sup>E. P. Hartouni, A. S. Moore, A. J. Crilly, B. D. Appelbe, P. A. Amendt, K. L. Baker, D. T. Casey, D. S. Clark, T. Döppner, M. J. Eckart, J. E. Field, M. Gatu Johnson, G. P. Grim, R. Hatarik, J. Jeet, S. M. Kerr, J. Kilkenny, A. L. Kritcher, K. D. Meaney, J. L. Milovich, D. H. Munro, R. C. Nora, A. E. Pak, J. E. Ralph, H. F. Robey, J. S. Ross, D. J. Schlossberg, S. M. Sepke, B. K. Spears, C. V. Young, and A. B. Zylstra, *Nat. Phys.* **19**, 72 (2023).
- <sup>15</sup>P. Chang, R. Betti, B. K. Spears, K. S. Anderson, J. Edwards, M. Fatenejad, J. D. Lindl, R. L. McCrory, R. Nora, and D. Shvarts, *Phys. Rev. Lett.* **104**, 135002 (2010).
- <sup>16</sup>T. Döppner, D. Callahan, O. Hurricane, D. Hinkel, T. Ma, H.-S. Park, L. Berzak Hopkins, D. Casey, P. Celliers, E. Dewald, T. Dittrich, S. Haan, A. Kritcher, A. MacPhee, S. L. Pape, A. Pak, P. Patel, P. Springer, J. Salmonson, R. Tommasini, L. Benedetti, E. Bond, D. Bradley, J. Caggiano, J. Church, S. Dixit, D. Edgell, M. Edwards, D. Fittinghoff, J. Frenje, M. Gatu Johnson, G. Grim, R. Hatarik, M. Havre, H. Herrmann, N. Izumi, S. Khan, J. Kline, J. Kruer, G. Kyrala, O. Landen, F. Merrill, J. Moody, A. Moore, A. Nikroo, J. Ralph, B. Remington, H. Robey, D. Sayre, M. Schneider, H. Streckert, R. Town, D. Turnbull, P. Volegov, A. Wan, K. Widmann, C. Wilde, and C. Yeaman, *Phys. Rev. Lett.* **115**, 055001 (2015).
- <sup>17</sup>V. Gopalaswamy, C. A. Williams, R. Betti, D. Patel, J. P. Knauer, A. Lees, D. Cao, E. M. Campbell, P. Farmakis, R. Ejaz, K. S. Anderson, R. Epstein, J. Carroll-Nellenbeck, I. V. Igumenshchev, J. A. Marozas, P. B. Radha, A. A. Solodov, C. A. Thomas, K. M. Woo, T. J. B. Collins, S. X. Hu, W. Scullin, D. Turnbull, V. N. Goncharov, K. Churnetski, C. J. Forrest, V. Y. Glebov, P. V. Heuer, H. McClow, R. C. Shah, C. Stoeckl, W. Theobald, D. H. Edgell, S. Ivancic, M. J. Rosenberg, S. P. Regan, D. Bredesen, C. Fella, M. Koch, R. T. Janezic, M. J. Bonino, D. R. Harding, K. A. Bauer, S. Sampat, L. J. Waxer, M. Labuzeta, S. F. B. Morse, M. Gatu-Johnson, R. D. Petrasso, J. A. Frenje, J. Murray, B. Serrato, D. Guzman, C. Shulderberg, M. Farrell, and C. Deeney, *Nat. Phys.* **20**, 751–757 (2024).



- <sup>18</sup>K. Churnetski, K. M. Woo, W. Theobald, C. Stoeckl, L. Ceurvorst, V. Gopalaswamy, H. Rinderknecht, P. V. Heuer, J. Knauer, C. Forrest, I. Igumenshchev, S. Ivancic, M. Michalko, R. Shah, A. Lees, R. Bahukutumbi, R. Betti, C. Thomas, S. Regan, J. Kunimune, C. Wink, P. Adrian, M. Gatu Johnson, and J. Frenje, *High Energy Density Phys.* **52**, 1–17 (2024).
- <sup>19</sup>S. Atzeni and J. Meyer-ter Vehn, *The Physics of Inertial Fusion: Beam Plasma Interaction, Hydrodynamics, Hot Dense Matter* (Oxford Science Publications, 2004).
- <sup>20</sup>O. Hurricane, P. Patel, R. Betti, D. Froula, S. Regan, S. Slutz, M. Gomez, and M. Sweeney, *Rev. Mod. Phys.* **95**, 025005 (2023).
- <sup>21</sup>W. Doughton, B. J. Albright, S. M. Finnegan, B. M. Haines, J. L. Kline, J. P. Sauppe, and J. M. Smidt, *Phys. Plasmas* **30**, 012704 (2023).
- <sup>22</sup>Z. Fan, J. Liu, B. Liu, C. Yu, and X. T. He, *Phys. Plasmas* **23**, 010703 (2016).
- <sup>23</sup>G. S. Fraley, E. J. Linnebur, R. J. Mason, and R. L. Morse, *Phys. Fluids* **17**, 474 (1974).
- <sup>24</sup>D. Wu, X. T. He, W. Yu, and S. Fritzsche, *High Power Laser Sci. Eng.* **6**, e50 (2018).
- <sup>25</sup>B. Spears, D. Hicks, C. Velsko, M. Stoyer, H. Robey, D. Munro, S. Haan, O. Landen, A. Nikroo, and H. Huang, *J. Phys.: Conf. Ser.* **112**, 022003 (2008).
- <sup>26</sup>S. Atzeni and A. Caruso, *Il Nuovo Cimento B* **80**, 71 (1984).
- <sup>27</sup>J. Daligault and J. Simoni, *Phys. Rev. E* **100**, 043201 (2019).
- <sup>28</sup>P. Springer, O. Hurricane, J. Hammer, R. Betti, D. Callahan, E. Campbell, D. Casey, C. Cerjan, D. Cao, E. Dewald, L. Divol, T. Doeppner, M. Edwards, J. Field, C. Forrest *et al.*, *Nucl. Fusion* **59**, 032009 (2019).
- <sup>29</sup>B. Cheng, P. A. Bradley, S. M. Finnegan, and C. A. Thomas, *Nucl. Fusion* **61**, 096010 (2021).
- <sup>30</sup>M. Temporal, V. Brandon, B. Canaud, J. Didelez, R. Fedosejevs, and R. Ramis, *Nucl. Fusion* **52**, 103011 (2012).